Electron-phonon relaxation rates in InGaAs–InP and HgCdTe–CdTe quantum wells

Augusto M. Alcalde and Gerald Weber

Citation: Journal of Applied Physics **85**, 7276 (1999); doi: 10.1063/1.370544
View online: http://dx.doi.org/10.1063/1.370544
View Table of Contents: http://scitation.aip.org/content/aip/journal/jap/85/10?ver=pdfcov
Published by the AIP Publishing

Electron-phonon relaxation rates in InGaAs–InP and HgCdTe–CdTe quantum wells

Augusto M. Alcalde[a)]
Instituto de Física, Universidade Estadual de Campinas, Caixa Postal 6165, 13083-970 Campinas SP, Brazil

Gerald Weber
Faculdade de Engenharia, Universidade São Francisco, 13251-900 Itatiba SP, Brazil

(Received 30 November 1998 accepted for publication 8 February 1999)

We calculate electron-LO-confined and interface-phonon scattering rates in $In_{1-x}Ga_xAs$–InP and $Hg_{1-x}Cd_xTe$–CdTe quantum wells considering the influence of nonparabolicity on the energy subbands. A simple $\mathbf{k}\cdot\mathbf{p}$ model is used to take into account this nonparabolicity and a reformulated dielectric continuum slab model is employed to describe the confined phonon modes. We find that the subband nonparabolicity increases the scattering rates significantly for all transitions and that this effect is more pronounced as transitions from higher subbands are involved. We show that this behavior can be understood in terms of the phonon wave vector, the density of final states and the electron-phonon overlap. © *1999 American Institute of Physics.* [S0021-8979(99)01410-3]

I. INTRODUCTION

The study of low-dimensional systems that includes semiconductor alloys mobilizes at the moment important theoretical and experimental efforts.[1,2] Particularly important is $In_{1-x}Ga_xAs$ since its optical gap it is very close to the optimum wavelength for optical communication. Additionally $Hg_{1-x}Cd_xTe$ quantum wells look promising for high efficient infrared detectors.[3,4] In both materials, the lattice parameters as well as the energy gap and other physical parameters can be adjusted by an appropriate chose of alloy composition.

Electron-phonon interaction in polar semiconductor quantum wells attracted a great amount of interest over the last years due to its importance for electronic and optic properties. For instance, the cooling of optically excited carriers on the picosecond time scale is primarily governed by the scattering of electrons by polar-optical phonons and reliable values for these scattering rates in realistic structures are needed for numerical and experimental studies of their properties. Particular interest was directed towards LO-phonon confinement which affects significantly the scattering rates in quantum wells.

In general, the use of dielectric continuum models for phonon description is well established[5] and scattering rates calculated with such models compare successfully with experimental results.[6,7] However, a question which has not yet been properly addressed is how strongly the subband nonparabolicity affects the intra- and intersubband scattering rates in quantum wells. In previous works,[8,9] we demonstrate that in materials that do not present great nonparabolicity such as $GaAs–Al_xGa_{1-x}As$ the inclusion of a realistic band description produces significant changes in the electron-phonon scattering rates. However, the band description used in these works[10] fails for materials with strong nonparabolicity. The purpose of the present work is to study the influence of subband nonparabolicity on intra- and intersubband scattering rates in materials where the coupling between bands produce strong deviations from parabolicity, like $In_{1-x}Ga_xAs$–InP and $Hg_{1-x}Cd_xTe$–CdTe quantum wells.

II. THEORY

Several theoretical models were proposed, in various degrees of complexity, to take into account the effect of nonparabolicity in the electronic band structure.[11–13] The main difference between those models is the form of the energy dispersion relation describing the subband nonparabolicity. In several works, the nonparabolicity has been included in the $E-\mathbf{k}$ dispersion relation by expressing the energy as a series expansion until order k^4 in the electron wave vector

$$E=\frac{\hbar^2k^2}{2m^*}(1-\gamma k^2), \tag{1}$$

where γ is the nonparabolicity parameter, this model is particulary appropiate for the scattering rates calculations in materials with weak nonparabolicity.[8,9] In strong nonparabolicity, this model cannot be applied since some parameters such as energy effective masses can diverge.[14] We chose an energy dispersion relation based on a two-band $\mathbf{k}\cdot\mathbf{p}$ model, which is thought to adequately represent the subband of highly nonparabolic quantum wells,[13] several properties of this systems have been studied using this dispersion relation[15,16]

$$k^2=\frac{2m^*}{\hbar^2}E(1+\alpha E)=\frac{2m^*}{\hbar^2}F(E), \tag{2}$$

where E is the total electron energy, m^* is the band edge mass, and α the nonparabolicity parameter. With $k^2=k_\parallel^2+k_z^2$ we have at the bottom of the subband $(k_\parallel^2=0)$,

a)Electronic mail: alcalde@ifi.unicamp.br

$$F(E_z)=\frac{\hbar^2 k_z^2}{2m^*}=E_z(1+\alpha E_z). \tag{3}$$

Following the models of electron-phonon interaction in mixed crystals with two-mode behavior discussed by Nash *et al.*[17] and Ridley,[18] we consider a binary compound $A^1_{1-x}A^2_xB$, with two modes A^1B-like (label 1), and A^2B-like (label 2) and supose that frequencies in the corresponding binary compounds are very different, thus the mixing between these two modes will be small. For the deduction of the further phonon scattering rates expressions, we consider the coupling Fröhlich parameters in a multimode theory given by Nash *et al.*[17]

The electron-LO-confined phonon scattering rates are obtained from the Fermi Golden Rule and with the well known electron-confined-phonon interaction Hamiltonian (Fröhlich interaction).[19] In final form, the scattering rates for an electron initially in a state k_i to the final state k_f accompanied by the emission of an optical phonon of frequency ω_{LO} is given by

$$W_{k_i\to k_f}=\frac{\lambda^2}{4\pi\hbar L}\frac{2m^*}{\hbar^2}\sum_n |G_n|^2\frac{L^2}{Qa_nL^2+b_n}\times\{1+4\alpha[F(E_z)+\hbar\omega^*]\}^{1/2}, \tag{4}$$

where

$$Q=\pm\left\{\frac{2m^*}{\hbar^2}[F(E_{zf})-F(E_{zi})\pm\hbar\omega^*]\right\}, \tag{5}$$

here the upper sign corresponds to intrasubband transitions, while the lower sign corresponds to intersubband transitions. For phonon emission, we define

$$\hbar\omega^*=\hbar\omega_{\mathrm{LO}}\{\alpha\hbar\omega_{\mathrm{LO}}[1+4\alpha F(E_z)]^{1/2}\}, \tag{6}$$

where $F(E_z)$ is related to the z component of the final (initial) electron wave vector for intrasubband (intersubband) transitions, and G_n is the electron-phonon overlap integral. Further parameters in Eq. (4) were defined in previous works.[9,20,21] The LO frequencies $\omega_{\mathrm{LO}(1,2)}$ are now determined by the quadratic equation obtained from the two-mode dielectric function $\epsilon(\omega)$, with $\epsilon=0$. For the description of the confined phonon modes, we used the corrected slab model[22] which gives scattering rates very close to the phenomenological[23] and microscopical models[24] and compares successfully with experimental results.[6,7]

The scattering rates for emission of interface modes in the $\mathbf{k}\cdot\mathbf{p}$ approximation can be determined from the electron-interface-phonon interaction Hamiltonian[19] and the nonparabolic dispersion relation (2)

$$W_{k_i\to k_f}=\frac{\hbar\omega_{\xi\mu(q_\parallel)}e^2}{4\epsilon_0\hbar}\frac{2m^*}{\hbar^2}\frac{f^2(Q)|G_n(Q)|^2}{2Q}\times\{1+[4\alpha F(E_z)+\hbar\omega^*]\}^{1/2}, \tag{7}$$

where $\omega_{\xi\mu}$ is the interface phonon frequency, ϵ_0 is the permitivity of vacuum, the subscript ξ refers to the symmetric or antisymmetric parity, and μ the possible solution of the interface-phonon dispersion equations, which give three interface normal mode frequencies: $\omega_{\xi,1}$ and $\omega_{\xi,2}$ originating from the A^1B-like modes and the A^2B-like modes of the $A^1_{1-x}A^2_xB$ region and $\omega_{\xi,B}$ originating from the barrier region. Figures 1(a) and 1(b) show the concentration dependence of the interface modes, for $\mathrm{In}_{1-x}\mathrm{Ga}_x\mathrm{As}$–InP and $\mathrm{Hg}_{1-x}\mathrm{Cd}_x\mathrm{Te}$–CdTe quantum wells, respectively. The index $s(a)$ indicates symmetric (antisymmetric) modes. For additional details and definitions of the remaining parameters of the electron-phonon Hamiltonian, we refer the reader to the work of Mori and Ando.[19]

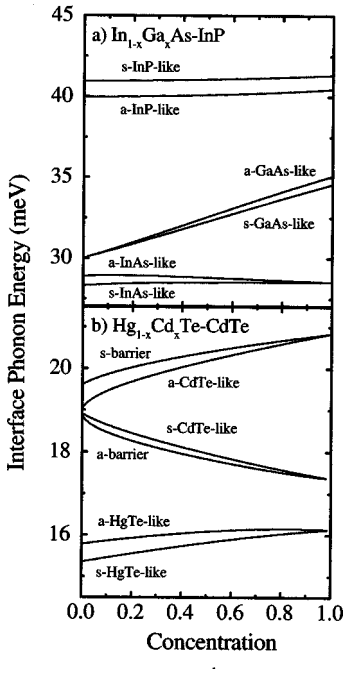

FIG. 1. Interface phonon energy in terms of concentration x for (a) $\mathrm{In}_{1-x}\mathrm{Ga}_x\mathrm{As}$–InP and (b) $\mathrm{Hg}_{1-x}\mathrm{Cd}_x\mathrm{Te}$–CdTe quantum wells. Interface modes are evaluated for $L=100$ Å.

For intrasubband transitions, we assume that the electron has just enough energy to emit one optical phonon and for intersubband transitions that the electron is initially at the bottom of the subband. We express our results as an average scattering rate $W=p_W W^{(W)}_{k_i\to k_f}+p_B W^{(B)}_{k_i\to k_f}$, where p_W (p_B) is the probability of finding the electron initially in the well (barrier) subband. This procedure is necessary because the effective masses as well as the nonparabolicity parameters in the well are different from those of the barrier.

It is important to point out that the expression for the scattering rates given by Eqs. (4) and (7) are deduced following the Fermi Golden Rule and the $\mathbf{k}\cdot\mathbf{p}$ dispersion relation (2), any additional supposition regarding the model used to describe the vibrational modes or to the method used to calculate the nonparabolic confinement energies it was used for its deduction.

In order to obtain the electron energy levels and wave functions, we use the model proposed by Nag and Mukhopadhyay.[13] The calculation scheme takes into account standard boundary conditions and energy dependent effective masses, which enters in the analysis when the envelope functions and its derivatives are matched at the heterojunction interface; the eigenvalue equations thus obtained are seemingly similar to those for the parabolic approach, with

TABLE I. Optical phonon parameters for the alloy $In_{1-x}Ga_xAs$ and $Hg_{1-x}Cd_xTe$. Barrier phonon parameters for the binary semiconductors InP and CdTe are also included.

Compound	LO-phonon energy (meV)	TO-phonon energy (meV)
InAs-like	$30.0-1.49x$	$27.34+1.17x$
GaAs-like	$30.0+6.75x$	$30.0+3.86x$
HgTe-like	$17.12-0.5749x-0.4318x^2$	$14.629+1.488x$
CdTe-like	$18.91+1.918x$	$18.91-1.56x$
InP	43.34	38.20
CdTe	20.82	17.35

the difference that the parameters k_z as much for the well as for the barrier, are now affected by the energy dependent effective masses. In this approach it is possible write the electron envelope wave function in the same functional form as for the simple parabolic subband model and therefore the overlap integrals exhibit the same form that for previous parabolic calculations;[20] therefore this model is particularly well suited for the comparative study of scattering rates for parabolic and nonparabolic electron subbands. In order to verify the efficiency of this nonparabolic band description, we applied the expressions (4) and (7) to $GaAs-Al_xGa_{1-x}As$ quantum wells, the rates obtained are in full agreement with our previous results.[8,9]

III. RESULTS AND DISCUSSION

The material parameters used in our calculations of scattering rates in $In_{1-x}Ga_xAs-InP$ quantum wells are taken from Ref. 17, for $Hg_{1-x}Cd_xTe-CdTe$ quantum wells we used the parameters reported in Ref. 25; complementary information was extracted from Refs. 26 and 27. Additionally, other composition dependent parameters, like phonon frequencies and bulk effective masses were obtained from fitting of experimental data. The expression for the nonparabolicity parameters in terms of the energy gap were obtained from Ref. 28. The phonon occupation number is assumed as $N_{LO}\sim 0$, which is valid for low temperatures. Relevant material parameters are summarized in Tables I and II.

In Figs. 2(a) and 2(b), we show the calculated scattering rates for intrasubband and intersubband transitions due to the emission of confined phonon modes as a function of the well width for $In_{0.53}Ga_{0.47}As-InP$ and $Hg_{0.6}Cd_{0.4}Te-CdTe$ quantum wells, respectively. The solid lines represent the scattering rates with the inclusion of subband nonparabolicity and the dashed lines are for the parabolic-band approximation. Note that the scattering rates are significantly increased in all transitions due to effects of nonparabolicity, except for intersubband transition in large InGaAs–InP quantum wells ($L>120$ Å), where the nonparabolic scattering rates decrease in comparison to the parabolic rates. The nonparabolic effects in the $Hg_{1-x}Cd_xTe-CdTe$ quantum well are more significant than for those of $In_{1-x}Ga_xAs-InP$, for both intrasubband and intersuband transitions. We observe that the effect of the subband on the scattering rates does not produce significant changes in the qualitative behavior from those of the parabolic-band approximation.

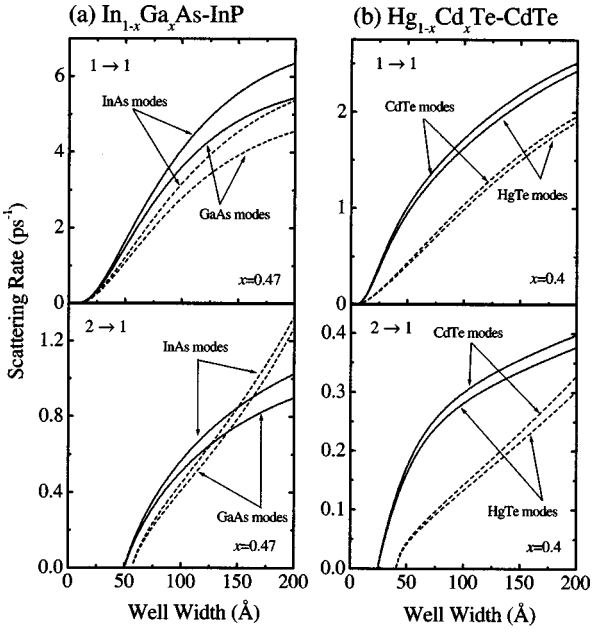

FIG. 2. Scattering rates for intrasubband and intersubband transitions for (a) $In_{1-x}Ga_xAs-InP$ and (b) $Hg_{1-x}Cd_xTe-CdTe$ quantum wells as a function of the well width. Solid lines are transition rates with subband nonparabolicity and dashed lines are for parabolic bands.

It is possible to identify three factors that are the mainly responsible for the variations in the transition rates when nonparabolic effects are included: the influence of the nonparabolic bands is equivalent to an increase of the quantum confinement, producing a larger electron-phonon overlap. Therefore, when the well width increases, the nonparabolic effects become less important. The second factor refers to the Fröhlich coupling which depends inversely with the wave vector of the emitted phonon (due to the nonparabolicity large phonon wave vectors are emitted), which implies in a reduction of the electron-phonon coupling. Finally, the nonparabolicity induces an increase in the density of final states. As the scattering rates are obtained by an integration over this density, this induces an enhancement in the scattering rates, which is especially important for intersubband transitions.

The fact that the scattering rates for intrasubband transitions including nonparabolicity increases for both quantum well systems studied, is a direct consequence of the increment of the electron-phonon overlap. For intersubband transitions, the larger density of final states also causes in the increase of these rates. However, in the intersubband transition (2→1) for the $In_{1-x}Ga_xAs-InP$ quantum well, we observe that from widths larger than 120 Å the parabolic rates

TABLE II. Band Structure parameters for the $In_{1-x}Ga_xAs-InP$ and $Hg_{1-x}Cd_xTe-CdTe$ quantum wells.

Compound	Effective mass (m_0)	Band gap energy (eV)
$In_{1-x}Ga_xAs$	$0.025+0.04x$	$1.425-1.337(1-x)+0.270(1-x)^2$
InP	0.079	1.423
$Hg_{1-x}Cd_xTc$	$-0.01305+0.1046x$[a]	$-0.25+1.59x+0.327x^3$
CdTe	0.091	1.667

[a]Valid for $x>0.15$.

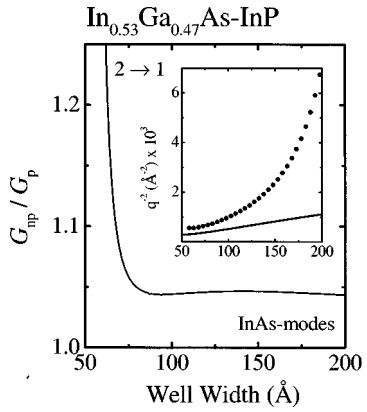

FIG. 3. Ratio of the nonparabolic and parabolic overlap integral for the intersubband transition in $In_{1-x}Ga_xAs-InP$ quantum well as a function of the well width. The inset shows the phonon wave vector contribution to the scattering rates for nonparabolic (solid line) and parabolic (dotted line) bands.

are increased; for these wide quantum wells, the confinement becomes weak and the effects of the nonparabolicity on the overlap integral are less important, in this situation the contribution of the larger vector of emitted phonon becomes dominant causing that the nonparabolic Fröhlich coupling diminishes. We illustrate this situation in the Fig. 3, where the ratio of the nonparabolic and parabolic overlap for the intersubband transition in $In_{1-x}Ga_xAs-InP$ quantum wells is shown; in the inset we plotted the nonparabolic (solid lines) and parabolic (dotted lines) inverse square of the emitted phonon wave vector in order to determine its influence on the scattering rates ($W \propto 1/q^2$). Only InAs-modes contribution is displayed. It is observed clearly that as the width of the well increases, the contribution of the nonparabolicity on the overlap integrals is less important, while the reduction of the rates due to the influence of the nonparabolic phonon wave vector becomes more evident. This behavior, allows to identify two regimes in the study of the nonparabolic effects, in situations with large confinement, the influence of the nonparabolic bands is reflected with more intensity on the overlap integrals, while in situations of weak confinement the role of the emitted phonon wave vector can be important.

The effects of the confinement can also be perceived when the concentration is varied; for the studied quantum wells, the increment of the concentration is equivalent to a decrease of the confinement, therefore it is expected that the nonparabolic effects in the rates are smaller when the concentration increases. This effect is seen clearly in the Fig. 4 where transition rates are shown in terms of the concentration and of the nonparabolicity parameter (upper horizontal axis) for a quantum well of fixed width ($L = 100$ Å). Note the dramatic effect induced by the nonparabolicity in situations of strong confinement. For example, for intersubband transition in $Hg_{1-x}Cd_xTe-CdTe$ quantum wells, the nonparabolic rates are approximately three times higher than the parabolic ones. For $In_{1-x}Ga_xAs-InP$, the nonparabolic effects diminishes almost completely when the concentration increases, while for $Hg_{1-x}Cd_xTe-CdTe$ some variations are still observed, revealing the strong nonparabolic characteristic of these materials. We observe of the Fig. 4(b) that for the

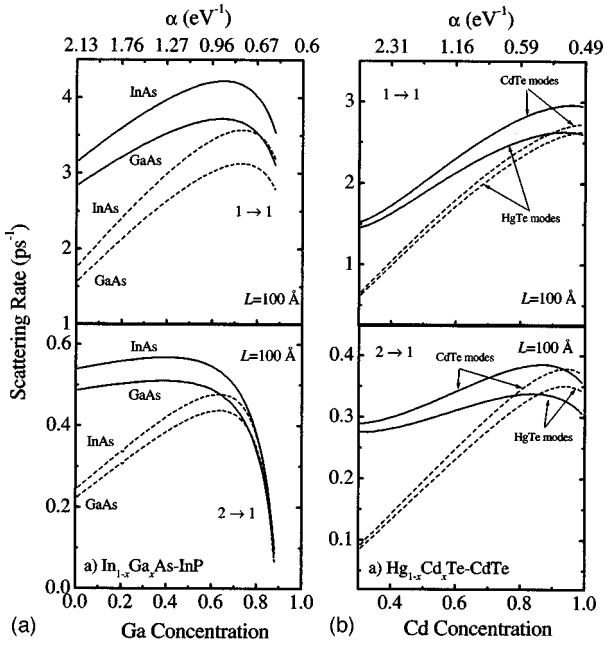

FIG. 4. Intrasubband and intersubband scattering rates for (a) $In_{1-x}Ga_xAs$ and (b) $Hg_{1-x}Cd_xTe-CdTe$ quantum wells as a function of the concentration x and nonparabolicity parameter for a fixed well width for 100 Å. Solid lines are transition rates with subband nonparabolicity and dashed lines are for parabolic bands.

intersubband transitions and for situations of weak confinement, the parabolic rates are larger than nonparabolic ones. This is a consequence of the dominant effects of the larger emitted nonparabolic wave vector which causes a decrease of the nonparabolic rates.

Figures 5(a) and 5(b) show the calculated scattering rates for intrasubband and intersubband transitions due to the

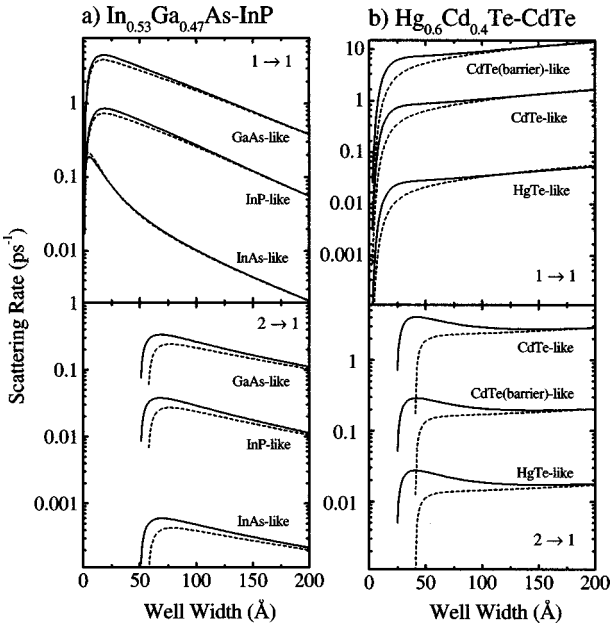

FIG. 5. Electron-interface phonon scattering rates for intrasubband and intersubband transitions for (a) $In_{1-x}Ga_xAs-InP$ and (b) $Hg_{1-x}Cd_xTe-CdTe$ quantum wells as a function of the well width. Solid lines are transition rates with subband nonparabolicity and dashed lines are for parabolic bands.

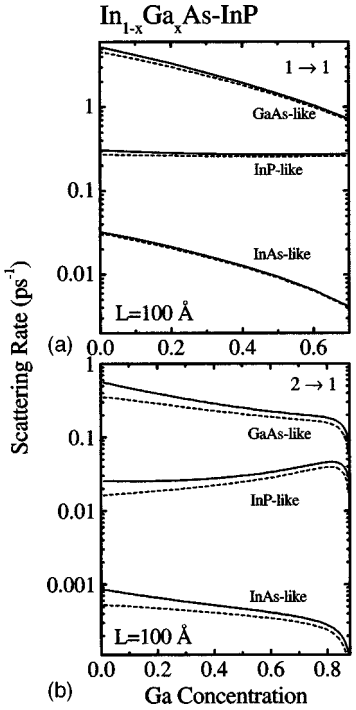

FIG. 6. Intrasubband and intersubband electron-interface phonon scattering rates for (a) $In_{1-x}Ga_xAs$ and (b) $Hg_{1-x}Cd_xTe$–CdTe quantum wells as a function of the concentration x for a fixed well width $L=100$ Å. Solid lines are transition rates with subband nonparabolicity and dashed lines are for parabolic bands.

emission of interface phonon modes as a function of the well width for $In_{0.53}Ga_{0.47}As$–InP and $Hg_{0.6}Cd_{0.4}Te$–CdTe quantum wells, respectively. The continuous lines represent the scattering rates with inclusion of subband nonparabolicity and the dashed lines are for the parabolic-band approximation. We show separately the individual contributions of the three interface modes. In general, we observe that no significant variations exist on the scattering rates due to the presence of nonparabolic bands. This low sensibility of the scattering rates with the electronic structure is a direct consequence of the weak electron-interface phonon coupling. The interface modes are strongly localized in the interfaces, while the nonparabolicity produces an additional localization of the electron wave function in the well region where the interface phonon potential is a minimum. Both for the intra- and intersubband transitions, the nonparabolic scattering rates are increased, specially in the intersubband case, but the scattering rates are otherwise not qualitatively different from those in the parabolic band approximation. This general enhancement of transition rates due to inclusion of nonparabolic bands results mainly from a larger density of states. For the $In_{0.53}Ga_{0.47}As$–InP system, we have numerically estimated that the nonparabolicity may cause a density of states variation of the order of 7% for intrasubband transitions and 35% for intersubband transitions, this explains why, the intersubband scattering rates are more affected with the inclusion of the subband nonparabolicity. Intra- and intersubband transition rates for $In_{1-x}Ga_xAs$–InP quantum wells in terms of Ga concentration are shown in the Fig. 6, the main features are similar to those described for the confined modes: the nonparabolic effects in the rates are smaller when the concentration increases, analogous behavior is obtained (not presented in this work) for $Hg_{1-x}Cd_xTe$–CdTe quantum wells.

IV. CONCLUSIONS

In conclusion, we have calculated the scattering rates for intrasubband and intersubband transitions due to electron-confined and interface-phonon interaction in quantum wells with strong subband nonparabolicity. We find that for intra and intersubband transitions the scattering rates are in general increased, except in some situations of low confinement. This general increase is more important in the case of confined modes. In particular, for higher subbands and larger electron confinement, the nonparabolicity effects becomes more important. We put into evidence that it is important to pay attention to the analysis of the overlap integral, since this parameter is not only sensitive to the variations of the electronic wave functions, but also to the electrostatic potential generated by the several phonon modes present in low-dimensional systems, therefore it is reasonable to suppose that the nonparabolic electron-phonon overlap not necessarily leads to an increment of the rates. Our results shows that the scattering rates are more sensitive to the variations caused by the nonparabolicity on the overlaps and density of states, only in few situations the emitted phonon wave vector has a significant contribution.

ACKNOWLEDGMENTS

The authors acknowledge financial support from FAPESP (96/5037-2), CNPq(522789/96-0), and Pepci/USF.

[1] C. R. M. de Oliveira *et al.*, Appl. Phys. Lett. **66**, 2998 (1995).
[2] K. Ogawa and Y. Matsui, Appl. Phys. Lett. **73**, 297 (1998).
[3] T. H. Myers, J. R. Meyer, and C. A. Hoffman, in *Quantum Wells and Superlattices for Long Wavelength Infrared Detectors*, edited by M. O. Manasreh (Artech House, Boston, 1993).
[4] *Narrow-gap II-VI Compounds for Optoelectronic and Electromagnetic Applications, Electronic Materials: 3*, 1st ed., edited by P. Capper (Chapman and Hall, London, 1997).
[5] H. Rücker, E. Molinari, and P. Lugli, Phys. Rev. B **45**, 6747 (1992).
[6] G. Weber and A. M. de Paula, Appl. Phys. Lett. **63**, 3026 (1993).
[7] A. M. de Paula and G. Weber, Appl. Phys. Lett. **65**, 1281 (1994).
[8] A. M. Alcalde and G. Weber, Solid State Commun. **96**, 763 (1995).
[9] A. M. Alcalde and G. Weber, Phys. Rev. B **56**, 9619 (1997).
[10] The $E-k$ dispersion relationship was expressed as a expansion up to second order in k^2: $E \propto k^2(1-\gamma k^2)$, where γ is the nonparabolicity parameter.
[11] D. F. Nelson, R. C. Miller, and D. A. Kleinman, Phys. Rev. B **35**, 7770 (1987).
[12] U. Ekenberg, Phys. Rev. B **36**, 6152 (1987).
[13] B. R. Nag and S. Mukhopadhyay, Phys. Status Solidi B **175**, 103 (1993).
[14] The condition $1-8\gamma m^*(E-V) \geqslant 0$ defines the limit of validity for the nonparabolic model used in Refs. 8 and 9; V is the bulk conduction-band offset.
[15] B. R. Nag, Appl. Phys. Lett. **59**, 1620 (1991).
[16] P. K. Chakraborty, J. Appl. Phys. **74**, 3246 (1993).
[17] K. J. Nash, M. S. Skolnick, and S. J. Bass, Semicond. Sci. Technol. **2**, 329 (1987).
[18] B. K. Ridley, *Electrons and phonons in semiconductor multilayers, Cambridge Studies in Semiconductors Physics and Microelectronic Engineering: 5* (Cambridge University Press, Cambridge, 1997).
[19] N. Mori and T. Ando, Phys. Rev. B **40**, 6175 (1989).

[20] G. Weber, A. M. de Paula, and J. F. Ryan, Semicond. Sci. Technol. **6**, 397 (1991).
[21] G. Weber and J. F. Ryan, Phys. Rev. B **45**, 11202 (1992).
[22] G. Weber, Phys. Rev. B **46**, 16171 (1992).
[23] K. Huang and B. Zhu, Phys. Rev. B **38**, 13377 (1988).
[24] E. Molinari *et al.*, Semicond. Sci. Technol. **7**, B67 (1992).
[25] P. W. Kruse, *Semiconductors and Semimetals* (Academic, London, 1981), Vol. 18, pp. 1–20.
[26] *Landolt-Börnstein, Numerical Data and Functional Relationships in Science and Technology, New Series*, edited by O. Madelung, M. Schulz, and H. Weiss (Springer Berlin, Heidelberg, 1982), Vol. 17(a).
[27] *Landolt-Börnstein, Numerical Data and Functional Relationships in Science and Technology, New Series*, edited by O. Madelung, M. Schulz, and H. Weiss (Springer, Berlin, Heidelberg, 1982), Vol. 17(b).
[28] V. A. Altschul, A. Fraenkel, and E. Finkman, J. Appl. Phys. **71**, 4382 (1992).